JOURNAL OF AIRCRAFT
Vol. 40, No. 3, May–June 2003

Six-Degree-of-Freedom Model of a Controlled Circular Parachute

Vladimir N. Dobrokhodov,* Oleg A. Yakimenko,† and Christopher J. Junge‡
U.S. Naval Postgraduate School, Monterey, California 93943-5106

The paper continues a series of publications devoted to modern advances in aerodynamic decelerator system technology started recently (*Journal of Aircraft*, Vol. 38, No. 5, 2001) and addresses the development of a six-degree-of-freedom model of a guided circular parachute. The paper reviews existing circular parachute models and discusses several modeling issues unresolved within the frame of existing approaches or completely ignored so far. These issues include using data obtained in the aerodynamic experiments and computational-fluid-dynamics modeling for both undistorted (uncontrolled) and distorted (controlled) canopy shapes, introducing and computing control derivatives, and providing comparison with the real flight data. The paper provides step-by-step development of the mathematical model of circular parachute that includes the basic equations of motion, analysis and computation of the aerodynamic forces and moments, and investigation with modeling of special modes observed in flight. It then introduces a new application of a two-step aerodynamic parameters identification algorithm that is based on comparison with two types of the air-drop data (uncontrolled set and controlled one). The paper ends with summary of the obtained results and proposes a vital direction for the further elaboration of the developed model.

Nomenclature

$\boldsymbol{A}_{6\times 6}$	=	apparent mass tensor
a_{pl}	=	dimension of a cubic payload container
$\{b\}$	=	body-fixed coordinate frame
C_D	=	aerodynamic drag coefficient of undisturbed canopy
C_m	=	aerodynamic moment coefficient of undisturbed canopy
C_n	=	yaw moment caused by yaw acceleration
$C_n^{\bar{l}}$	=	control moment coefficient
C_n^r	=	damping moment coefficient
$\boldsymbol{F}$	=	vector of external force
$\boldsymbol{F}^{a/d}$	=	total aerodynamic force vector
$\boldsymbol{F}_{\text{canopy}}$	=	aerodynamic force vector of undisturbed canopy
$\boldsymbol{F}_{\text{risers}}$	=	force vector caused by the change in riser length
$\boldsymbol{G}$	=	gravitation vector caused by Earth's gravity g
I_{jj}	=	moments of inertia about axes of $\{b\}$
I_{jj}^i	=	moments of inertia of the ith component about axes of $\{b\}$
$\tilde{I}_{jj}^i$	=	central moments of inertia of the ith component in its centroid-fixed axes
$k_{C_{D0}}, k_{C_{D\alpha}}, k_{C_m}$	=	optimization parameters
k_{mn}	=	empirical coefficients for symmetrical (undisturbed) canopy used to compute apparent mass tensor's components
l_B	=	distance between the origin of $\{b\}$ and the top of payload
$\bar{l}_k$	=	relative length of kth actuator ($\bar{l} \in [0; 1]$)
$l_{\max}$	=	length of actuated pneumatic muscle actuators
$l_{\text{PMA}} = l_{\min}$	=	nominal length of pneumatic muscle actuators
l_{SL}	=	length of suspension lines
$\boldsymbol{M}$	=	vector of external moment
$\boldsymbol{M}_{\text{canopy}}$	=	aerodynamic moment vector of undisturbed canopy
$\boldsymbol{M}_G^i$	=	moments caused by the weight of the ith component when being translated to the center of gravity of the whole system
$\boldsymbol{M}_{\text{risers}}$	=	vector of the moment caused by the change in riser length
$\boldsymbol{M}^{a/d}$	=	total aerodynamic moment vector
m	=	total mass of the system
m_a	=	mass of air trapped by the canopy
m_i	=	mass of the ith component
n	=	number of actuators activated ($n \in \{1, 2\}$)
$\boldsymbol{P}_{CP}$	=	location of the center of pressure in $\{b\}$
P_{PMA}	=	pressure in pneumatic muscle actuators
$\boldsymbol{P}_u = [x_u, y_u, z_u]^T$	=	position of the real system in $\{u\}$
$\hat{\boldsymbol{P}}_u$	=	position of the model in $\{u\}$
q	=	dynamic pressure
R_p	=	radius of inflated parachute
R_0	=	nominal or reference radius of uninflated canopy
${}_b^u R$	=	rotation matrix from $\{b\}$ to $\{u\}$
S_0	=	canopy's reference area
T	=	total energy
T^{ADS}	=	kinetic energy of the parachute
T^{air}	=	kinetic energy of surrounding air
t_f	=	flight (descent) time
$\{u\}$	=	local tangent plane coordinate frame
$\boldsymbol{V} = [u, v, w]^T$	=	inertial velocity vector
$\boldsymbol{V}_a = [u_a, v_a, w_a]^T$	=	airspeed vector
$\boldsymbol{V}_u = [V_x, V_y, V_z]^T$	=	inertial velocity vector measured in $\{u\}$
W_u	=	wind vector measured in $\{u\}$
z_G	=	z coordinate of the system's center of gravity in $\{b\}$
z_i	=	z coordinate of the ith component's centroid in $\{b\}$
$\alpha, \alpha_{\text{sp}}$	=	angle of attack, spatial angle of attack
α_{mn}	=	apparent mass tensor's components
β	=	side-slip angle
ε	=	canopy shape ratio
ρ	=	air density

Received 7 July 2002; presented as Paper 2002-4613 at the AIAA Atmospheric Flight Mechanics Conference, Monterey, CA, 6–9 August 2002; revision received 6 January 2003; accepted for publication 14 January 2003.

*National Research Council Research Associate, Department of Aeronautics and Astronautics. Member AIAA.
†Research Associate Professor, Department of Aeronautics and Astronautics. Associate Fellow AIAA.
‡Lieutenant Commander of the U.S. Navy, Department of Aeronautics and Astronautics. Member AIAA.

τ = actuator's transition time
φ, ϑ, ψ = Euler angles
$\mathbf{\Omega} = [p, q, r]^T$ = vector of angular velocity

Subscripts

i = component of an aerial delivery system ($i \in \{1, 2, 3, 4\}$)
j = axes of $\{b\}$ ($j \in \{x, y, z\}$)
k = actuator number ($k \in \{1, 2, 3, 4\}$)
m, n = row and column of 6×6 tensor vector

Introduction

PARACHUTES have been the simplest and cheapest devices used for the delivery of materials, people, and vehicles ever since their first recorded use by Jacques Garnering who jumped from a balloon over Paris in 1797. However, this very simplicity makes their aerodynamics very difficult to model. Specifically, the parachute not only deflects surrounding air, but also adopts its shape, which is dictated by the airflow generated by the canopy. Furthermore, lack of streamlining during control activation makes turbulent rather than laminar flow dominate the parachute's aerodynamics.

Significant research on flat circular parachute modeling has been done over the past 60 years by researchers in the U.S., Europe, and Russia. However, no complete model of a controlled circular parachute has been developed so far (whereas a number of efficient techniques addressing the control of maneuverable parachutes like parafoil exists). Moreover, existing high-degree-of-freedom models of circular noncontrolled parachutes lack verified nonlinear aerodynamics and use mostly empirical values for the apparent mass terms (see Refs. 1–22).

The main contribution of the work reported here is the development of a controlled model of a six-degree-of-freedom (DoF) circular parachute. This was done by applying a nonlinear system identification algorithm to refine the computational-fluid-dynamics (CFD) values of the aerodynamic coefficients. The critical idea was to first identify the uncontrolled model aerodynamics and use the resulting estimates to identify the controlled model aerodynamics. Another important step was to subtract the influence of the wind when determining the controlled model. This approach was made possible by the richness of the flight data set,[23,24] that is, data for both uncontrolled and controlled drops were available.

A detailed analysis of the circular parachute modeling problem discussed in the literature has identified two shortcomings inherent in existing methods: 1) estimation of apparent mass terms is done empirically for axisymmetric shapes; 2) the only aerodynamics considered are those of a fully deployed and symmetric canopy.

Based on Henn's[1] work introducing apparent mass coefficients (1944), several authors developed mathematical models of a different degree of complexity to investigate the dynamic behavior of parachutes (e.g., see Ref. 2). Different empirical values for two apparent masses were used in these studies. In 1962 Lester[3] rederived basic equations of motion showing that Henn's equations were erroneous. At the same time Ibrahim[4,5] has conducted the first exhaustive analysis of the apparent mass and moment of inertia terms of cup-shaped bodies in unsteady incompressible flow. He was also the first one who showed that resulting parachute dynamic performance is sensitive to the values of these terms. This study initiated the scientific debate on the extent of influence of the apparent mass terms on the stability of a descending system. Many authors[13–17] concluded that neglecting nonlinear terms and the stochastic nature of parachute dynamics would lead to completely inaccurate modeling and also stressed the need for experimental determination of the apparent mass terms. An attempt to use theoretical apparent mass and moments-of-inertia coefficients based on those related to the air displaced by ellipsoids of revolution moving in a potential fluid was made also.[12] One of the latest experimental studies[14,15] suggests that apparent masses and moments of inertia (hereafter referred to jointly as the apparent mass tensor terms) are the functions of a spatial angle of attack and depending on acceleration might significantly exceed the theoretical ones.

With regard to aerodynamics of the fully deployed canopies with a symmetric shape, various authors have shown that the nonlinear nature of basic aerodynamic terms is a function of the angle of attack. For instance, in Ref. 16 authors discuss parameter identification using flight-test data, where they point out that the dependence of aerodynamic terms on the angle of attack is highly nonlinear unlike those of an aircraft. Many of papers[12,14,15,17] include sufficient data for fully deployed canopies and a variety of flight conditions. (Similar to the aircraft aerodynamics the majority of available data has been obtained on the base of wind-tunnel experiments.) However, the results reported employ predetermined symmetric canopy shapes. The aerodynamics of a distorted canopy has not been considered.

In summary, over the past 40 years a consensus on the lack of accurate dynamic modeling of apparent-mass effects and nonlinear aerodynamics of distorted canopies has emerged.

The complexity of parachute motion has also been confirmed by the extensive amount of real air-drop experiments.[21–24] First, it has been verified that strongly non-linear nature of the parachute aerodynamics is determined by three major factors: flight conditions, canopy shape, and geometry of "parachute-payload" system [thereafter referred to as an aerial delivery system (ADS)]. Thus, assuming that the material geometry does not change during flight leads to the conclusion that aerodynamic forces and moments depend on canopy shape, spatial angle of attack, and dynamic pressure.

Second, the distortion of the axisymmetric canopy shape rules out employing the well-established analytical results used to determine the apparent mass tensor for axisymmetric canopy. This problem has not been resolved. Therefore, based on preliminary results provided by CFD techniques[25] and our own analysis, several assumptions have been made to model canopy distortion caused by control inputs. In particular, it was assumed that the number of canopy shapes caused by control inputs are finite and known.

At the same time there is an essential yaw rotation caused by canopy shape distortion when even a small difference between the length of two adjacent control inputs is presented. Therefore, the control input performance strongly affects the whole system dynamics. Hence, the controlled parachute model should properly consider it.

Finally, the descent rate depends not only on air density but also on control inputs through the canopy shape distortion that was also observed during the real drops. Therefore, the model of the controlled flat circular parachute should include six degrees of freedom with an appropriate description of apparent mass tensor, aerodynamics, and control system dynamics.

This paper is organized as follows. The next section addresses the development of a six-DoF parachute model. It contains the detailed discussion of the mathematical issues involved, beginning with analysis of the basic equations of motion, followed by computation of aerodynamic forces and moments, and ending with the modeling of some special modes observed in the flight test. The following section discusses verification of the parachute model using a two-step parameter identification technique. The paper ends with the conclusions. The Appendix contains mass–geometry datum for a generic ADS consisting of a G-12 parachute and an A-22 container, which was used for modeling.

Model Development

Definitions and Assumptions

In this section we discuss the development of a circular parachute model. The specific parameters and geometry of descending system used were those of a G-12 parachute. The G-12 is a 150-m^2 nylon cargo parachute with 64 suspension lines (SL)[26] (Fig. 1). The A-22 delivery container was selected as a prototype cargo box. This 1.82-m^3 almost cubic container has a payload capacity of nearly a ton and is commonly used with the G-12 by the U.S. Army.

The following controlled ADS architecture is considered. All lines are assembled into eight link assembles (see Fig. 1). Each pair of assembles is attached to one of four risers. At the other end the risers are coupled to the payload at four dispersed points (see Fig. 2). By design these risers allow controlling the parachute by

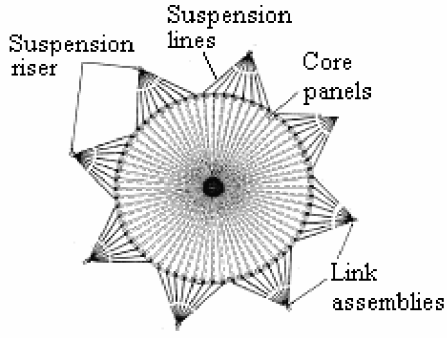

Fig. 1 G-12 parachute canopy.

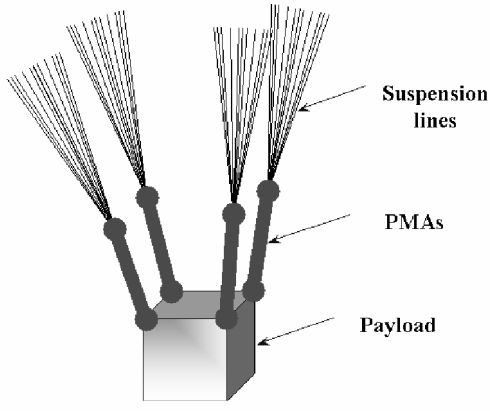

Fig. 2 Payload rigging.

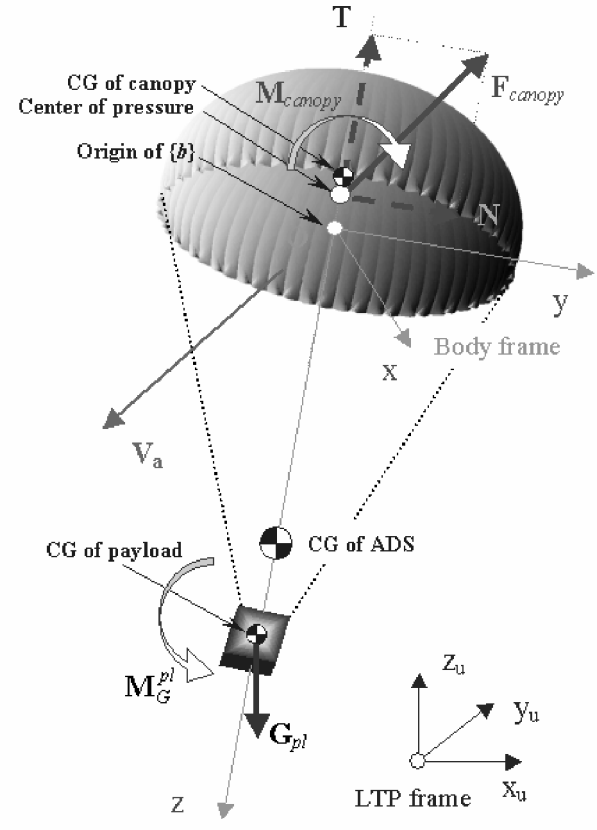

Fig. 3 System of axes and definition of aerodynamic terms.

lengthening one or two adjacent actuators and hence disturbing the symmetric shape of the canopy. The pneumatic muscle actuators (PMA) developed by Vertigo, Inc.,[27] are modeled and used in this study as a prototype of the control risers.

Two Cartesian coordinate systems have been chosen to describe ADS motion (see Fig. 3).

Linear position of the ADS is computed with respect to a local tangent plane $\{u\}$. Its positive y direction is aligned with local North, the positive x direction points East, and the positive z direction points up.

All other computations are performed in the body-fixed coordinate frame $\{b\}$. Its origin is attached to the center of the open-end plane of the canopy. The x and y body axes lie in the plane parallel to the canopy's base, and z is aligned with the imaginary axis extending toward the centroid of the payload.

It is worth mentioning that in different aerohydrodynamic studies the origin of $\{b\}$ is sometimes placed at the canopy's centroid. The undisturbed canopy is always assumed to be a planetary ellipsoid, but it can have a different ratio of minor and major axes. That makes the location of the origin of $\{b\}$ to be conditional from the concrete parachute design. Moreover the z coordinate of the canopy centroid can be determined only approximately because in the general case there is no analytical formula for ellipsoidal shells. Despite the fact that originally the six-DoF model presented in this paper was also developed with this setup of the frame $\{b\}$, it was later on redone with the origin at the center of the open-end plane of the canopy to make equations of motion more universal.

For simplicity we will skip subscript b in the further analysis, assuming that all variables and aerodynamic coefficients when applicable are defined in $\{b\}$.

The following assumptions mostly adopted from the Tory and Ayres paper[12] were used to develop the model:

1) Because of the predetermined architecture, the parachute and payload are considered to be rigidly connected to each other (Fig. 2).

2) During the air drop, these two rigidly connected parts are assumed to experience only gravity and aerodynamic forces.

3) The canopy experiences all aerodynamic forces and moments about its center of pressure.

4) The aerodynamic forces generated by the payload are negligible.

5) Undistorted canopy has an axial symmetry about the z axis.

Distortion of the canopy's shape (caused by the lengthening of one or two adjacent risers) introduces asymmetric forces and moments allowing steering of the ADS in a certain direction in a horizontal plane. Moreover, it obviously makes ADS nonsymmetrical. (One plane of symmetry still remains, but its location is not constant with respect to the body frame.) In this study however we will additionally assume that the effect of risers lengthening and canopy distortion from the standpoint of changing tensors of inertia and apparent masses is negligibly small. Therefore even for a controlled circular parachute these two tensors will be assumed to have the same form as for uncontrolled (symmetrical) parachute.

Aerial Delivery System Geometry

Figure 4 introduces a set of parameters defining the parachute's geometry. Numbers 1 . . . 4 denote the ADS's components: canopy, rigging (suspension) lines, actuators (PMAs), and payload. The position of their centroids z_i are determined with respect to the body frame origin (point O on Fig. 4).

On this figure $R_p = \frac{2}{3}R_0$ denotes the radius of inflated parachute, and a_{pl} denotes the dimension of a container (without loss of generality all three dimensions of a cargo container were considered to be the same).

As just mentioned, the shape of undisturbed canopy is a half of a planetary ellipsoid (hemispheroid), meaning that it is circular in plan when viewed along the z direction and elliptical when viewed from the side. The ratio of the minor to major axes (canopy shape ratio) will be denoted as ε. Tory and Ayres[12] reported that this ratio for a flat circular canopy is typically equal to 0.5. Other researchers (e.g., see Refs. 14–17) assumed canopy to be a hemisphere ($\varepsilon = 1$). For the ADS at hand, ε is equal to 0.82.

Basic Six-Degree-of-Freedom Equations

Following basic analytical mechanics principles, the total energy T of a whole descending system relative to body frame can be

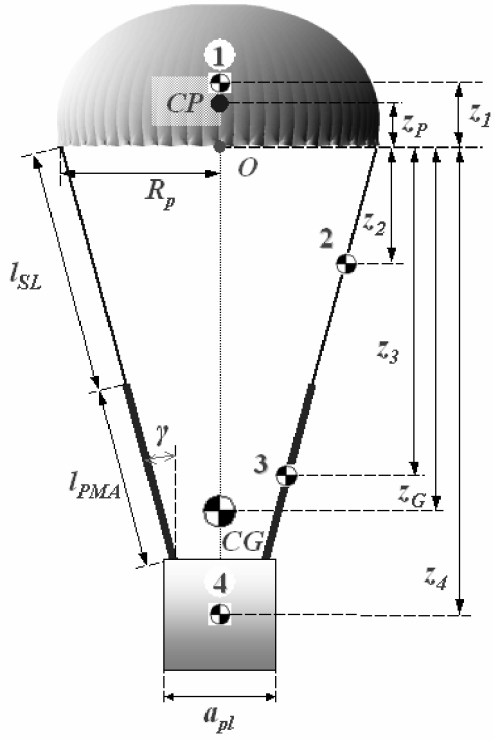

Fig. 4 ADS geometry.

given by

$$T = T^{\text{ADS}} + T^{\text{air}} \tag{1}$$

The expressions for T, T^{ADS}, and T^{air} can be found in Ref. 16.

For an ideal fluid the kinetic energy can be determined in terms of velocity potential. However, it is common practice[16] to assume that the kinetic energy of real fluid can be defined similarly. Using the Lagrange approach, the basic equations of motion for the parachute–air system can be obtained. The most general form of these equations in $\{b\}$ is

$$\frac{\mathrm{d}}{\mathrm{d}t}\left(\frac{\partial T}{\partial \boldsymbol{V}}\right) + \boldsymbol{\Omega} \times \left(\frac{\partial T}{\partial \boldsymbol{V}}\right) = \boldsymbol{F} \tag{2}$$

$$\frac{\mathrm{d}}{\mathrm{d}t}\left(\frac{\partial T}{\partial \boldsymbol{\Omega}}\right) + \boldsymbol{\Omega} \times \left(\frac{\partial T}{\partial \boldsymbol{\Omega}}\right) + \boldsymbol{V} \times \left(\frac{\partial T}{\partial \boldsymbol{V}}\right) = \boldsymbol{M} \tag{3}$$

where after substituting the expression for kinetic energy of the body and the air into Eqs. (2) and (3) and applying appropriate apparent mass tensor for a symmetric body, and some algebra, the final form of equations of motion will appear to be as follows:

$$\boldsymbol{F} = \begin{bmatrix} (m+\alpha_{11})(\dot{u} - vr) + (m+\alpha_{33})wq + (K+\alpha_{15})(\dot{q} + rp) \\ (m+\alpha_{11})(\dot{v} + ur) - (m+\alpha_{33})wp - (K+\alpha_{15})(\dot{p} - qr) \\ (m+\alpha_{33})\dot{w} - (m+\alpha_{11})(uq - vp) - (K+\alpha_{15})(p^2+q^2) \end{bmatrix} \tag{4}$$

$$\boldsymbol{M} = \begin{bmatrix} (I_{xx}+\alpha_{44})\dot{p} - (K+\alpha_{15})(\dot{v} - wp + ur) - (I_{yy}+\alpha_{44}-I_{zz}-\alpha_{66})qr + (\alpha_{33}-\alpha_{11})vw \\ (I_{yy}+\alpha_{44})\dot{q} + (K+\alpha_{15})(\dot{u} + wq - vr) + (I_{yy}+\alpha_{44}-I_{zz}-\alpha_{66})pr - (\alpha_{33}-\alpha_{11})uw \\ (I_{zz}+\alpha_{66})\dot{r} + (I_{yy}-I_{xx})pq \end{bmatrix} \tag{5}$$

(An example of step-by-step derivation of these equations can be found for example in Ref. 16.)

In Eqs. (4) and (5),

$$m = \sum_{i=1}^{4} m_i$$

denotes the mass of the system that includes the mass of canopy m_1, rigging lines m_2, actuators m_3, and payload m_4,

$$K = \sum_{i=1}^{4} m_i z_i = m z_G$$

where z_G is the static c.g. of the overall ADS with respect to the point O (see Fig. 4). The other notations denote the diagonal components of ADS's inertia tensor I_{xx}, I_{yy}, I_{zz} and apparent mass tensor's components α_{mn}. The only asymmetry left in these equations is caused by a possible asymmetry of payload. (I_{xx} in general might not be equal to I_{yy}.) (Computation of both tensors is considered in details in the following subsections.)

Equations (4) and (5) are very similar to those used to model a rigid-body motion [$\boldsymbol{F} = m\boldsymbol{V} + m(\boldsymbol{\Omega} \times \boldsymbol{V})$ and $\boldsymbol{M} = \boldsymbol{I}\dot{\boldsymbol{\Omega}} + \boldsymbol{\Omega} \times \boldsymbol{I}\boldsymbol{\Omega}$], and in vector form they can be rewritten as follows:

$$\boldsymbol{F} = \boldsymbol{M}_m \dot{\boldsymbol{V}} + \boldsymbol{\Lambda}_c \hat{\boldsymbol{M}}_m, \qquad \boldsymbol{M} = \boldsymbol{I}\dot{\boldsymbol{\Omega}} + \boldsymbol{H}_c \hat{\boldsymbol{I}} + \boldsymbol{M}_{\text{cr}} \tag{6}$$

In the latter expression

$$\boldsymbol{M}_m = \text{diag}\{m + \alpha_{11}, m + \alpha_{11}, m + \alpha_{33}\}$$

$$\boldsymbol{\Lambda}_c = \begin{bmatrix} -vr & wq & \dot{q} + rp \\ ur & -wp & qr - \dot{p} \\ vp - uq & 0 & -(p^2+q^2) \end{bmatrix}$$

$$\hat{\boldsymbol{M}}_m = [m + \alpha_{11}, m + \alpha_{33}, K + \alpha_{15}]^T$$

$$\boldsymbol{I} = \text{diag}\{I_{xx} + \alpha_{44}, I_{yy} + \alpha_{44}, I_{zz} + \alpha_{66}\}$$

$$\boldsymbol{H}_c = \begin{bmatrix} wp - ur - \dot{v} & -qr & vw \\ wq - vr + \dot{u} & pr & -uw \\ 0 & 0 & 0 \end{bmatrix}$$

$$\hat{\boldsymbol{I}} = [K + \alpha_{15}, I_{yy} + \alpha_{44} - I_{zz} - \alpha_{66}, \alpha_{33} - \alpha_{11}]^T$$

$$\boldsymbol{M}_{\text{cr}} = [0, 0, (I_{yy} - I_{xx})pq]^T$$

Being resolved with respect to $\dot{\boldsymbol{V}}$ and $\dot{\boldsymbol{\Omega}}$, Eqs. (6) yield

$$\dot{\boldsymbol{V}} = \boldsymbol{M}_m^{-1}(\boldsymbol{F} - \boldsymbol{\Lambda}_c \hat{\boldsymbol{M}}_m), \qquad \dot{\Omega} = I^{-1}(\boldsymbol{M} - \boldsymbol{H}_c \hat{I} - \boldsymbol{M}_{\text{cr}}) \tag{7}$$

The attitude of the ADS is determined by the Euler angles φ, ϑ, and ψ. The relation between vector $\boldsymbol{\Omega}$ and Euler angles is found in the usual way[28,29]:

$$\begin{bmatrix} \dot{\phi} \\ \dot{\theta} \\ \dot{\psi} \end{bmatrix} = \begin{bmatrix} 1 & \sin\phi \,\text{tg}\,\theta & \cos\phi \,\text{tg}\,\theta \\ 0 & \cos\phi & \sin\phi \\ 0 & \sin\phi(1/\cos\theta) & \cos\phi(1/\cos\theta) \end{bmatrix} \boldsymbol{\Omega} \tag{8}$$

The local tangent plane coordinates $\boldsymbol{P}_u = [x_u, y_u, z_u]^T$ of the origin of $\{b\}$ can be obtained employing corresponding rotation matrix ${}^u_b R$:

$$\dot{\boldsymbol{P}}_u = {}^u_b R \boldsymbol{V} \tag{9}$$

Computation of Moments of Inertia

The static mass center and moments of inertia are determined based on the weight and dimensions of each component.

First, the z coordinate of each component centroid with respect to one of its surfaces $\tilde{z}_i$ and individual central moments of inertia for each component in the axes of correspondent centroid $\tilde{I}^i_{jj}$ were derived. (Magnitudes of z_i then can be computed with account of $\tilde{z}_i$.)

Table 1 Relevant formulas of moments of inertia for parachute components

Component	Canopy (1)	Suspension lines (2) and PMAs (3)	Payload (4)
$\tilde{z}_i = \lvert\overrightarrow{BC}\rvert$	$-\frac{R_p}{2}\varepsilon^{0.83}$	$\frac{L\cos\gamma}{2}$	$\frac{a_{\text{pl}}}{2}$
$\tilde{I}^i_{aa} = \tilde{I}^i_{bb}$	$0.248 m_1 R_p^2 e^{0.52\varepsilon}$ $0.246 m_1 R_p^2 e^{\varepsilon}\left(I^1_{xx} = I^1_{yy}\right)$	$\frac{m_i}{2}\left[\frac{L^2(1+\cos^2\gamma)}{12} + R_*^2\right]$	$\frac{m_4 a_{\text{pl}}^2}{6}$
$\tilde{I}^i_{cc}$	$\frac{2}{3} m_1 R_p^2 (1 + 0.143\,\ln\varepsilon)$	$m_i\left(\frac{L^2\sin^2\gamma}{12} + R_*^2\right)$	$\frac{m_4 a_{\text{pl}}^2}{6}$

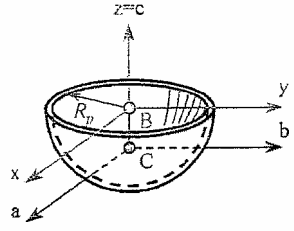

Fig. 5a Canopy (1).

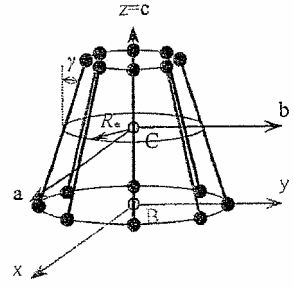

Fig. 5b Suspension lines (2) and PMAs (3).

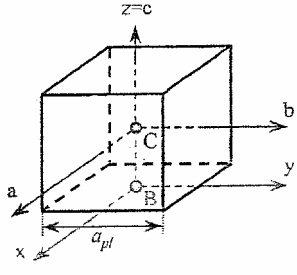

Fig. 5c Payload (4).

Table 1 contains formulas for each component. Figures 5a–5c show the components. Although formulas for a hemispherical shell and a solid cube (payload) are well known (for example, see Ref. 30), the formulas for a hemispheroidal shell and for a frustum right circular cone shell formed by SLs or PMAs are original. Approximate formulas for a hemispheroidal shell were specifically derived to match real values in the range of $\varepsilon \in [0.5; 1]$. (Exact cumbersome formulas for a hemispheroidal shell can be found for instance in Ref. 31.)

In Table 1 R_* is a radius of the shell measured at the z coordinate of its centroid. ($R_* = R_p - l_{\text{SL}}\sin\gamma/2$ for SLs and $R_* = a_{\text{pl}}/\sqrt{2} + l_{\text{PMA}}\sin\gamma/2$ for PMAs.) The cone half-angle γ for the considered ADS configuration can be computed from the geometric relation $\sin\gamma = (R_p - a_{\text{pl}}/\sqrt{2})(l_{\text{SL}} + l_{\text{PMA}})^{-1}$.

The individual inertia components were then transferred to the origin of $\{b\}$ using the parallel axis theorem

$$I^i_{jj} = \tilde{I}^i_{jj} + m_i z_i^2, \qquad i = 1, \ldots, 4 \tag{10}$$

Finally, the moments of inertia for the whole ADS were computed as a sum of inertias of corresponding ADS components

$$I_{jj} = \sum_{i=1}^{4} I^i_{jj}$$

The numerical values for the moments of inertia of each component of a generic ADS are given in Table A4 in the Appendix. Here it can be stated that although the major contributions into I_{xx} and I_{yy} moments of inertia are obviously caused by the payload (more than 98%), moment I_{zz} is formed basically by the parachute itself (canopy, SLs, and PMAs) with a minor influence of payload (less than 15%). That shows why it is reasonable to neglect the effect of ADS asymmetry while lengthening risers. Another feature is that the symmetry of the cargo box with respect to the axis z simplifies Eqs. (7) zeroing vector $\boldsymbol{M}_{\text{cr}}$.

Apparent Mass Terms

Similar to the rigid-body mass tensor, the apparent (virtual) mass tensor $\boldsymbol{A}$ has $6{\cdot}6 = 36$ elements, and in a real fluid these can all be unique. For an ideal fluid, however, $\boldsymbol{A}$ is a symmetrical tensor, leaving a maximum of 21 distinct terms. In the case of a body with two planes of symmetry and coordinate frame origin located somewhere on the axis of symmetry, tensor $\boldsymbol{A}$ can be further reduced to the following form:

$$\boldsymbol{A} = \begin{bmatrix} \alpha_{11} & 0 & 0 & 0 & \alpha_{15} & 0 \\ 0 & \alpha_{22} & 0 & \alpha_{24} & 0 & 0 \\ 0 & 0 & \alpha_{33} & 0 & 0 & 0 \\ 0 & \alpha_{24} & 0 & \alpha_{44} & 0 & 0 \\ \alpha_{15} & 0 & 0 & 0 & \alpha_{55} & 0 \\ 0 & 0 & 0 & 0 & 0 & \alpha_{66} \end{bmatrix} \tag{11}$$

Here the first three diagonal elements represent apparent masses of the air virtually stagnant within and around (below) the canopy, the next three are correspondent apparent moments of inertia, and the off-diagonal air mass/inertia elements contribute to the coupling motion.

Because of axial symmetry of the circular canopy, $\alpha_{22} = \alpha_{11}$, $\alpha_{55} = \alpha_{44}$, and $\alpha_{24} = -\alpha_{15}$. That leaves only three distinct elements, which are $\alpha_{11}, \alpha_{33}, \alpha_{44}, \alpha_{15}$, and α_{66}. [That is why dynamic equations have their appearance, Eqs. (4) and (5)].

In the earlier studies to represent a flow around a fully deployed canopy, the latter was represented as a spheroid. In this case the reference air mass and moments of inertia correspond to those of the air displaced by the body

$$m_a = m_a^s = \tfrac{4}{3}\pi\rho R_p^3\varepsilon \tag{12}$$

$$I^{\text{air}}_{xx} = \tfrac{1}{5} m_a R_p^2(1+\varepsilon^2), \qquad I^{\text{air}}_{zz} = \tfrac{2}{5} m_a R_p^2 \tag{13}$$

(see conventions of Table 1).

Today it is a usual practice to refer to the air trapped within a hemisperoid. In this case air mass makes the half of spheroid

$$m_a = 0.5 m_a^s \tag{14}$$

and formulas for the moments of inertia are the same as Eqs. (13). If needed to be computed with respect to centroid axes, the z coordinate

for the hemispheroid's centroid equal to $z_P = -\frac{3}{8}\varepsilon R_p$ needs to be taken into consideration.

Generally speaking, apparent mass terms depend on the canopy's configuration, porosity, acceleration, and spatial angle of attack. For instance, Ibrahim[4,5] showed that apparent masses can drop their values more than 20 times with the porosity increased from 0 to 40%. Apparent moments of inertia also decrease their values by the factor of 2.75. In their experimental study Yavuz and Cockrell[14] and Yavuz[15] demonstrated strong dependence of the angle of attack on especially α_{33}. (It decreases 4.5 times with increase of the angle of attack from 0 to 40 deg.) They also revealed a strong dependence of apparent mass terms from appropriate accelerations showing that they can change as much as by a factor of five while experiencing steady acceleration. With regard to the latter study, however it is unclear how the dependence from acceleration can be taken into account. First, the parachute does not experience a constant acceleration during descent. According to the flight-test data available, accelerations during descent of a fully deployed parachute oscillate around zero. But even the value at zero acceleration cannot be implemented because all dependences have a first-order discontinuity at this point so that the values differ as much as three times when approaching to the steady-state descent (zero acceleration) from negative to positive acceleration, not mentioning that the data were obtained for the small rigid models of a hemisphere canopy. Second, the physical values of apparent masses obtained at zero acceleration when being scaled to the whole ADS make no sense because they exceed those of ADS itself (see the following).

Therefore in the present study the authors followed all other major studies and considered all apparent mass terms to depend explicitly on the air density only. All other possible effects were represented by constant coefficients:

$$\alpha_{11} = k_{11} m_a, \qquad \alpha_{33} = k_{33} m_a, \qquad \alpha_{44} = k_{44} \tilde{I}_{xxa}$$

$$\alpha_{66} = k_{66} \tilde{I}_{zza}, \qquad \alpha_{15} = k_{15} m_a z_P \tag{15}$$

As opposed to other studies[17] where expression $l_B = \sqrt{[(l_{SL} + l_{PMA})^2 - R_p^2]}$ (see Fig. 4) was used as a reference length, z_P representing the distance from frame $\{b\}$ origin to the point of application of the translational apparent mass component (canopy's center of pressure) was used because of the sense of Eqs. (4) and (5).[4,5,9–11,14]

Following Ref. 17, coefficients in Eqs. (15) were taken to be as follows: $k_{11} = 0.5$, $k_{33} = 1.0$, $k_{44} = 0.24$, and $k_{15} = 0.75$. [Actually the values given are slightly different from the values in Ref. 17 because they were recomputed to match notations (13) and (14).]

For the ADS at hand with $m_a = 472$ kg ($\rho = 1$ kgm^{-3}), the following expressions are valid: $\alpha_{11} = 236$ kg (~22% of m), $\alpha_{33} = 472$ kg (~44% of m), $\alpha_{44} = 1600$ kgm^2 (less than 0.5% of I_{xx}), and $\alpha_{15} = 707$ kgm (~3% of K). By looking at these numbers, it becomes clear that α_{11} and α_{33} are evidently of most importance. The difference between them affects the dynamic behavior of the system [see Eqs. (5)].

To give an impression what coefficients were used by the other researches, Table 2 contains some data on the major research in the area for the past 60 years.

Henn[1] was the first to perform a stability analysis with account of apparent masses. For a spheroid as a reference body, he took 0.5 as a baseline values for both coefficients α_{11} and α_{33} and varied them within the shown range. Eighteen years later Ludwig and Heins[2] increased the baseline value and extended the range. At the end of the 1960s based on experimental research by Ibrahim,[4,5] White and Wolf[8] solved the five-DoF equations of motion using approximately the same values for apparent masses and introduced apparent moment of inertia α_{44}. Tory and Ayres[12] implemented theoretical values computed for the potential flow around spheroid. Not only did they use erroneous equations, but their modeling data seemed to not match the results of experiment.

The beginning of the 1980s was a new era of circular parachute modeling. Eaton[13] and other research teams[14,16,17] developed the right set of six-DoF equations and performed stability analysis. Eaton's coefficients if referred to the mass of a hemispheroid rather than a spheroid would give the values of 0.4 and 0.8 for the apparent masses, which is fairly close to those of Doherr and others.[16,17]

In spite of the results of experimental work of Yavuz and Cockrell[14] and Yavuz[15] showing completely different scale for apparent mass terms, it looks like everybody is continuing using the classical set of Doherr (e.g., see Refs. 18–20).

The present study was not aimed at tuning these coefficients, and so a classical set of apparent mass terms was used here also. However the authors would like to address this issue in the future. It also explains why element α_{66} was left in equations notwithstanding that for undisturbed canopy it is always neglected. For undisturbed canopy it contributes to the damping of yaw oscillations, and so authors also normalized it as shown in Eqs. (15) for the future study, letting k_{66} however to be zero here.

Computation of Forces and Moments

Aerodynamic Forces and Moments for Undisturbed Canopy

The total external force and moment acting on the system (Fig. 3) are caused by the aerodynamic effects and the weight of each system component. Thus, we can write

$$\boldsymbol{F} = \boldsymbol{F}^{a/d} + \boldsymbol{G}, \qquad \boldsymbol{M} = \boldsymbol{M}^{a/d} + \sum_i \boldsymbol{M}_G^i \tag{16}$$

where $\boldsymbol{G} = {}^u_b R^T [0, 0, mg]^T$ (the apparent (virtual) masses do not contribute to the weight of the system).

In turn, for controlled ADS

$$\boldsymbol{F}^{a/d} = \boldsymbol{F}_{\text{canopy}} + \boldsymbol{F}_{\text{risers}}, \qquad \boldsymbol{M}^{a/d} = \boldsymbol{M}_{\text{canopy}} + \boldsymbol{M}_{\text{risers}} \tag{17}$$

Let us address further in this subsection aerodynamic terms for undistorted canopy. Initial values of the dimensionless aerodynamic coefficients of a circular parachute were obtained from two sources. The basic shape of the aerodynamic curves for the undistorted canopy was adopted from Knacke,[26] whereas initial aerodynamic coefficient estimates were based on CFD results provided by Mosseev.[25]

The functional dependence of the aerodynamic coefficients on the angle of attack obtained by Mosseev is shown on Fig. 6.

On this figure $C_D(\alpha_{sp})$ denotes aerodynamic drag coefficient, and $C_m(\alpha_{sp})$ denotes total aerodynamic moment coefficient, both depending on the spatial angle of attack.

This spatial angle of attack α_{sp} and its components—angle of attack α and sideslip angle β—are shown on Fig. 7 and can be computed using $\{b\}$-frame components of an airspeed vector $\boldsymbol{V}_a$ as follows:

Table 2 Values of apparent mass coefficients

No.	Researcher	Year	Model	Origin of $\{b\}$	Ref. body	ε	k_{11}	k_{33}	k_{44}	k_{15}
1	Henn[1]	1944	Three DoF	O	Spheroid	0.5	**0.5** [0–0.6]	**0.5** [0–1.0]	——	——
2	Ludwig, Heins[2]	1962	Three DoF	O	Spheroid	0.5	**1.0** [0.6–1.4]	**1.0** [0.6–1.4]	——	——
3	White, Wolf[8]	1968	Five DoF	Sys. c.g.	Sphere	1	**0.7**	**0.7**	**0.23**	——
4	Tory, Ayres[12]	1977	Six DoF	Can. c.g.	Spheroid	0.5	**1.31**	**2.12**	**1.34**	——
5	Eaton[13]	1981	Six DoF	Can. c.g.	Spheroid	0.5	**0.2** [0–0.5]	**0.4** [0–1.0]	Unclear	——
6	Yavuz, Cockrell[14,15]	1981	Six DoF	Can. c.g.	Hemisphere	1	[1.31–6]	[2.12–10]	1.5–3.0	——
7	Cockrell, Doherr, Saliaris[16,17]	1981	Six DoF	O	Hemisphere	1	**0.5**	**1.0**	**0.24**	**0.75**
8	Present	2003	Six DoF	O	Hemispheroid	0.82	**0.5**	**1.0**	**0.24**	**0.75**

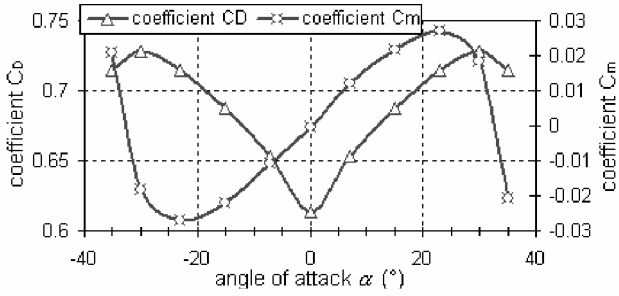

Fig. 6 G-12 parachute aerodynamics.

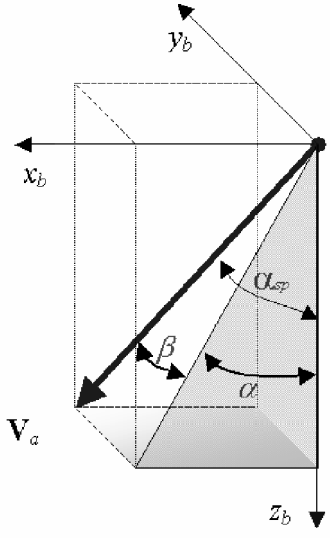

Fig. 7 Flight angles determination.

$$\alpha_{\text{sp}} = \cos^{-1}\left(\frac{w_a}{\sqrt{u_a^2 + v_a^2 + w_a^2}}\right) \tag{18}$$

$$\alpha = \tan^{-1}\left(\frac{u_a}{w_a}\right), \qquad \beta = \tan^{-1}\left(\frac{v_a}{\sqrt{u_a^2 + w_a^2}}\right) \tag{19}$$

The airspeed vector accounts for a wind vector $\boldsymbol{W}_u$ in the following manner:

$$\boldsymbol{V}_a = \boldsymbol{V} - {}^{u}_{b}R^T \boldsymbol{W}_u \tag{20}$$

Obviously the aerodynamic force vector $\boldsymbol{F}_{\text{canopy}}$ depends on the spatial angle of attack and dynamic pressure and can be presented as follows:

$$\boldsymbol{F}_{\text{canopy}} = C_D(\alpha_{\text{sp}}) q S_0 (\boldsymbol{V}_a / \|\boldsymbol{V}_a\|) \tag{21}$$

where $q = 0.5\rho\|\boldsymbol{V}_a\|^2$ is dynamic pressure; $\|\cdot\|$ denotes an Euclidian norm of vector; and $S_0 = \pi R_0^2$ is the canopy's reference area.

White and Wolf[8] showed that the longitudinal and the lateral motion of a parachute in glide plane are sufficiently uncoupled. Therefore, the longitudinal and lateral motion of a symmetric parachute can be studied separately, similar to the study of the aircraft linearized dynamics.[28,29] This leads us to assume additionally that the longitudinal and the lateral motion of a circular parachute in a glide plane are uncoupled.

This last assumption implies that roll and pitch motion of the ADS have the same moment characteristics, that is, $C_{\text{roll}} = C_m(\beta)$, $C_{\text{pitch}} = C_m(\alpha)$. Therefore, the vector of aerodynamic moment can be expressed as follows:

$$\boldsymbol{M}_{\text{canopy}} = 2q S_0 R_0 \begin{bmatrix} C_{\text{roll}} \\ C_{\text{pitch}} \\ C_n \end{bmatrix} \tag{22}$$

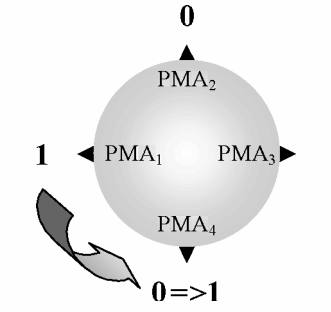

Fig. 8 Yaw rotation scheme.

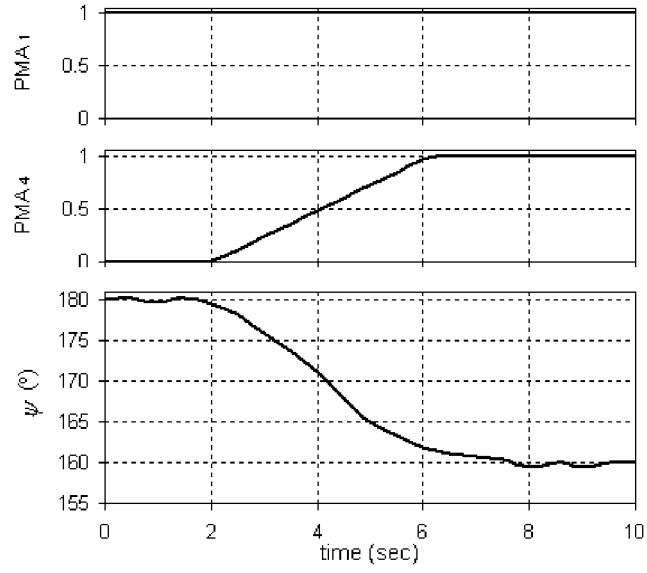

Fig. 9 Effect of changing riser length.

In Eq. (22) C_n denotes the yaw moment caused by yaw acceleration, and for a symmetric body it is equal to zero. However in case of transition of one of the risers from one state to another while one of the adjacent risers has been already lengthened, this moment is not equal to zero. The next subsection addresses this issue.

Yaw Moment Caused by Dynamic Asymmetry

As just mentioned, significant yaw rotation was observed during the flight tests when the length of the riser was changing while one of the adjacent risers has been already lengthened. Figure 8 clarifies this situation.

Here "0" stands for a shortened riser ($\bar{l}_k = 0$), and "1" denotes a lengthened riser ($\bar{l}_k = 1$), typically while riser transition (4 . . . 5 s) yaw angle of 15 . . . 20 deg was accrued (Fig. 9).

Therefore, if the kth riser undergoes transition the following relation is valid:

$$C_n = \text{sign}(\bar{l}_{k-1} - \bar{l}_{k+1}) C_n^{\bar{l}}(\bar{l}) \bar{l}_k + C_n^r r \tag{23}$$

In Eq. (23) $\bar{l}_k = (l_k - l_{\min})/(l_{\max} - l_{\min})$, and the difference $(\bar{l}_{k-1} - \bar{l}_{k+1})$ defines the sign of the moment.

By analyzing data from 20 flight tests, the functional dependence $C_n^{\bar{l}}(\bar{l})$ was found to be as presented on Fig. 10 and the coefficient C_n^r to be constant and equal to 2 s.

When $\bar{l}$ or $1 - \bar{l}$ is small, as happens at the very beginning and at the very end of the actuation process, the magnitude of the rotation is low because the canopy symmetry distortion is minimal. The rotation is at its highest at the middle of actuation process when the shape distortion is maximal (see Fig. 9).

Actuator Forces and Moments

Let us define now an effect of riser actuation.

Vertigo's PMA[27] used as a prototype of control riser is braided fiber tubes with neoprene inner sleeves that can be pressurized. In

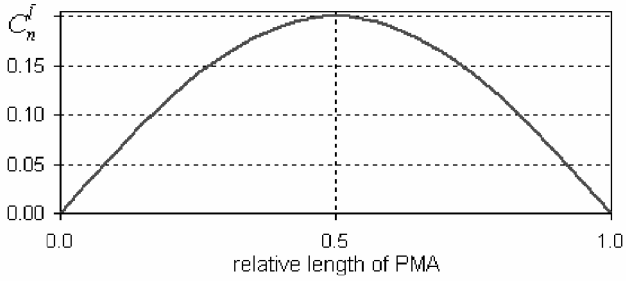

Fig. 10 Dependence $C_n^{\bar{l}}(\bar{l})$.

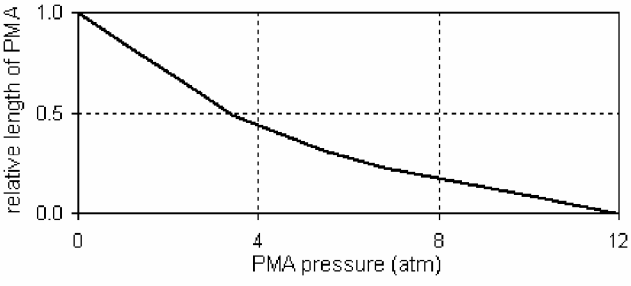

Fig. 11 Dependence $\bar{l}_{\mathrm{PMA}} = f(P_{\mathrm{PMA}})$.

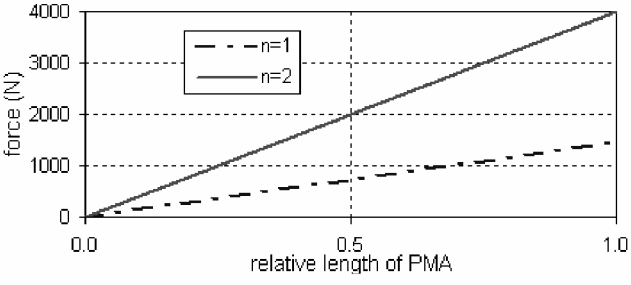

Fig. 12 Dependence $\|\boldsymbol{F}_{\mathrm{risers}}\| = f(\bar{l}, n)$.

the nominal state all PMAs are pressurized. Upon venting, PMA increases its length by approximately one third from $l_{\mathrm{PMA}} = l_{\min}$ to $l^*_{\mathrm{PMA}} = l_{\max} = l_{\mathrm{PMA}} + \Delta l_{\mathrm{PMA}}$ and compresses in diameter. [The dependence $\bar{l}_{\mathrm{PMA}} = f(P_{\mathrm{PMA}})$ where P_{PMA} stands for the PMA pressure is shown on Fig. 11]. This action "deforms" the parachute canopy creating an asymmetrical shape, essentially shifting the center of pressure and providing a drive or slip condition in the opposite direction of the control action. With four independently controlled actuators, two of which can be activated simultaneously, eight distinct control actions can be generated.

The change in the aerodynamic force caused by PMA activation $\boldsymbol{F}_{\mathrm{risers}}$ was modeled as a function of PMA's relative length $\bar{l}$, number of PMA actuated n, and involved actuation system dynamics with transition time τ[27]:

$$\|\boldsymbol{F}_{\mathrm{risers}}(t)\| = f(\bar{l}, n, \tau) \tag{24}$$

Figure 12 shows steady-state values of this dependence. In turn, the actuator moment can be computed as $\boldsymbol{M}_{\mathrm{risers}} = P_{\mathrm{CP}} \times \boldsymbol{F}_{\mathrm{risers}}$, where $P_{\mathrm{CP}} = [0, 0, z_P]^T$.

Model Identification

In the preceding section we outlined all steps involved in the development of the Six-DoF model for a controlled circular parachute. Next this model was compared with the flight-test data. This comparison revealed inadequacy of the data obtained by CFD analysis (see Fig. 6). Therefore, a standard nonlinear system identification technique[32] was applied to tune the CFD dependences $C^*_D(\alpha_{\mathrm{sp}})$ and $C^*_m(\alpha_{\mathrm{sp}})$ (see Fig. 13).

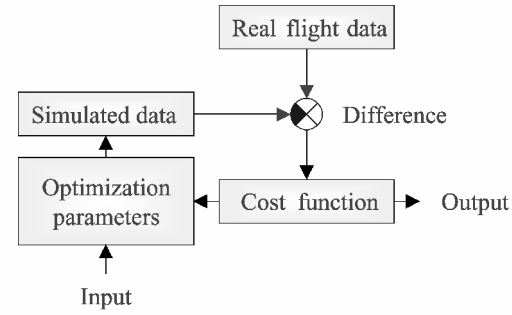

Fig. 13 Block diagram of the system identification technique.

First, expressions for $C_d(\alpha_{\mathrm{sp}})$ and $C_m(\alpha_{\mathrm{sp}})$ were presented in the following form:

$$C_D(\alpha_{\mathrm{sp}}) = k_{C_{D0}} \tilde{C}_{D_{\alpha=0}} + k_{C_{D\alpha}} \left[C^*_D(\alpha_{\mathrm{sp}}) - C^*_D(0) \right] \tag{25}$$

$$C_m(\alpha_{\mathrm{sp}}) = k_{C_m} C^*_m(\alpha_{\mathrm{sp}}) \tag{26}$$

yielding three optimization parameters $k_{C_{D0}}$, $k_{C_{D\alpha}}$, and k_{C_m}. The initial value of $\tilde{C}_{D_{\alpha=0}} = mg(qS_0)^{-1}$ was obtained from the obvious equation for a steady descent rate.

Second, an appropriate cost function was chosen:

$$J = \int_0^{t_f} \|\boldsymbol{P}_u(t) - \hat{\boldsymbol{P}}_u(t)\| \, \mathrm{d}t \tag{27}$$

where $\boldsymbol{P}_u(t)$ is the inertial position of ADS obtained in flight test, $\hat{\boldsymbol{P}}_u(t)$ denotes the estimated position of ADS obtained in simulation, and t_f stands for the flight time.

Therefore the objective of identification was to minimize cost function (27) by varying three parameters in Eqs. (25) and (26) (Fig. 13).

Because from the analysis of the flight-test data it became obvious that there was a significant difference in the ADS dynamics during controlled and uncontrolled drops, the identification algorithm was first applied to the data obtained from the uncontrolled drop. The resulting values of $k_{C_{D0}}$, $k_{C_{D\alpha}}$, and k_{C_m} were used then to initialize the second step, where the same technique was applied to a controlled drop. Whereas values of optimization parameters obtained in the first step provided estimates of ADS aerodynamics around zero angle of attack, their adjustment at the second step characterized ADS dynamics at higher angles of attack with nonzero control inputs. As a result, some averaged values were found to match both controlled and uncontrolled real-drop sets.

All two- and three-dimensional trajectories in this section are plotted in East–North–Up local tangent plane (LTP) coordinates.

Uncontrolled Model Identification

This subsection details results obtained by applying the identification technique to the uncontrolled drop data. Because the model assumes a fully deployed canopy, it was initialized at the point on the real-drop trajectory where the canopy was fully deployed.

Figures 14–16 contain the three- and two-dimensional plots of the trajectories, obtained in one of the real flight three-DoF and six-DoF simulations. (The three-DoF model of the parachute was used in the preliminary study.[21])

Note that the real trajectory has three points where the parachute's direction of motion changes more than 90 deg. This particular data set was selected because of the richness of the frequency spectrum of the parachute motion involved. Fig. 17 contains the wind profile for the same drop. It clearly indicates that both wind direction and its magnitude experience significant changes with time.

Because during the uncontrolled drop the angle of attack and sideslip angle are close to zero the value of k_{C_m} was set to zero. This choice implies that the amplitude of coning motion can differ from the flight-test data; however, its natural frequency does not depend on k_{C_m} for uncontrolled drops. Finally, the optimal values

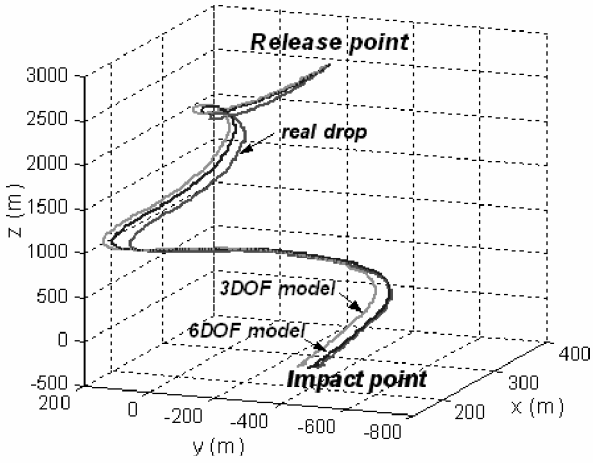

Fig. 14 Three-dimensional projections.

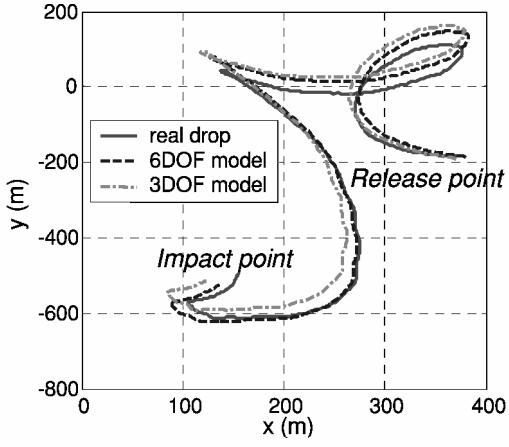

Fig. 15 Horizontal projection.

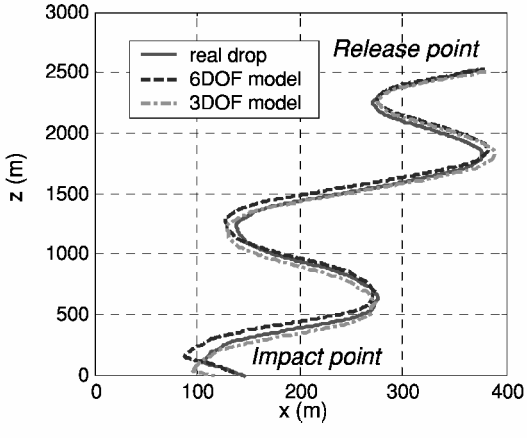

Fig. 16 Vertical projection.

$k_{C_{d0}}$ and $k_{C_{D_\alpha}}$ were obtained by determining a priori the range of their possible values from physical considerations and applying simple search techniques over the resulting grid of this parameter space.

Figures 18–20 include plots of the x, y, and z components of the inertial velocity obtained from the six-DoF model simulation and during the flight test. Analogous data are plotted for the three-DoF model. A conspicuous feature of the six-DoF model can be seen in the plots of the vertical or z component. (Figure 20 shows absolute values). Although the vertical component of the three-DoF model remains constant during the flight, the same component of the six-DoF model follows the flight-test data reasonably well. Therefore optimization over a set of two parameters gave fairly good results.

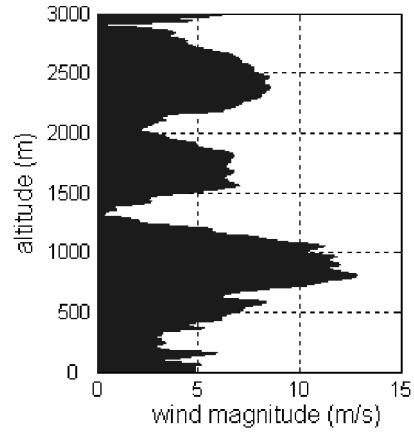

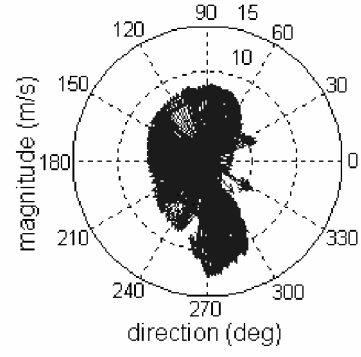

Fig. 17 Wind profile.

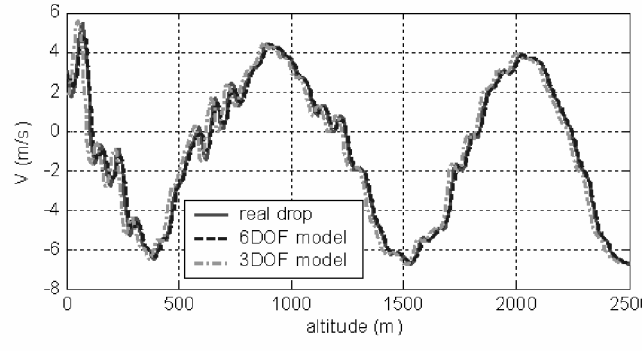

Fig. 18 Comparison of V_x components.

Figure 21 contains power spectrum density (PSD) plots for Euler angles (roll, pitch, and yaw) taken from the flight test and the six-DoF model run. Among dozens of methods available, the Multiple Signal Classification method developed by Schmidt[33] was applied. This method was chosen to demonstrate a general similarity between real and simulated data as well as to emphasize the matching of principal eigenfrequencies on the both sets of data.

Numerical values of these principal eigenfrequencies for each channel are depicted in Table 3.

Similar results for the principal eigenfrequencies were obtained independently for another set of ADS flight-test data using Welch's method as well.[34] That shows the consistency of ADS flight-test data taken in the presence of the different wind profiles, indicating that the data in Table 3 reflect the inherent motion of the ADS, and not the wind spectrum.

In turn, the wind spectrum characteristics for the real drop being analyzed are presented in Fig. 22. The results clearly show that the wind energy was concentrated around much higher frequency (1.9 Hz) rather than 0.11-Hz parachute's harmonic just seen.

The main conclusion to be drawn from spectral analysis is that the six-DoF model dynamics are sufficiently close to those of the actual system.

Controlled-Drop Dynamics Verification

To isolate the influence of control on the parachute aerodynamics, the following approach was used. First the wind profile measured during the controlled drop was used to simulate the uncontrolled model. Then this simulated data were subtracted from the flight-test data, and the result was used as an input data for the system identification algorithm. This looks reasonable because the control's influence on the descent rate is minor; hence, the new input data are supposed to approximate controlled drop in the absence of wind.

An example of trajectories at the presence of strong wind is shown in Fig. 23. By applying the described procedure, a contribution of control actions was received as a difference of two trajectories.

The result of the identification procedure for this case is depicted in Fig. 24. Here the "Control + NoWind" graph represents the position obtained by driving the six-DoF model with no wind and with control inputs recorded in the real drop. (The logic of the control algorithm is described in detail in Ref. 35.)

Finally, Fig. 25 compares controlled-drop trajectories obtained in simulation with double tuned aerodynamics and flight test.

Table 3 Eigenfrequencies

Euler angle	PSD rate, Hz	
	Real drop	Six-DoF model
Roll	0.109	0.114
Pitch	0.112	0.111
Yaw	0.12, 0.22, and 0.406	0.13, 0.22, and 0.41

Table 4 Values of optimization parameters

Optimization parameter	Initial value	Uncontrolled drop	Controlled drop
k_{CD0}	1	1.2	1.2
$k_{CD\alpha}$	1	1.005	1.25
k_{Cm}	1	0	0.6

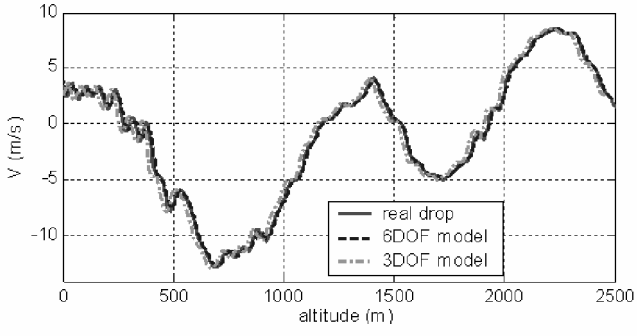

Fig. 19 Comparison of V_y components.

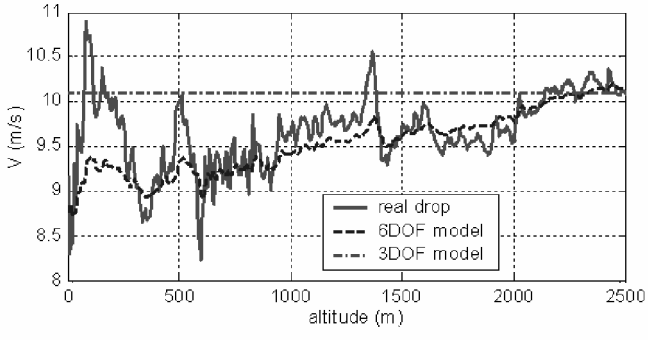

Fig. 20 Comparison of absolute values of V_z components.

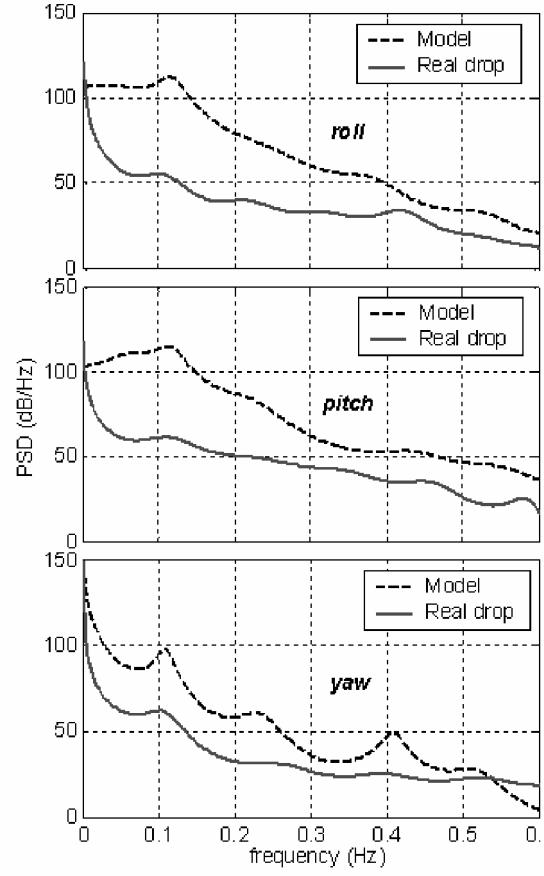

Fig. 21 Euler angles PSD analysis.

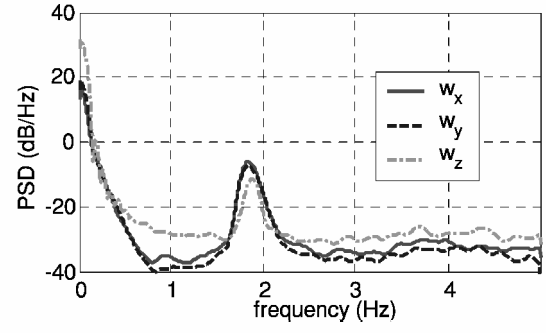

Fig. 22 Wind profile PSD.

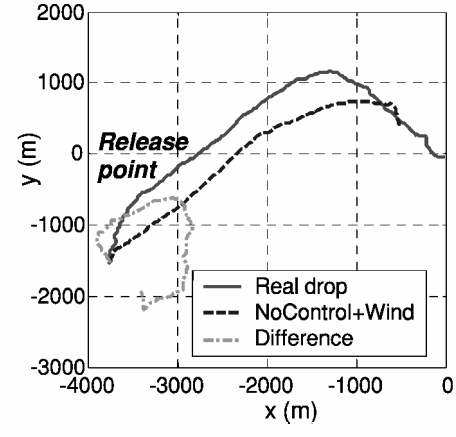

Fig. 23 On the control contribution.

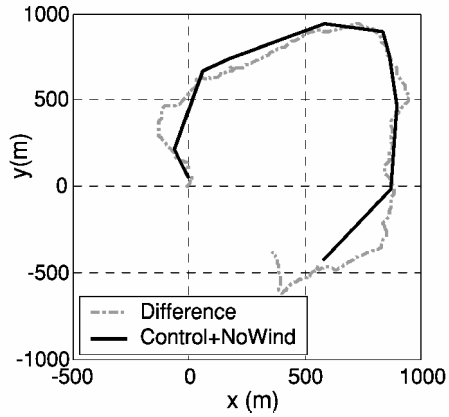

Fig. 24 Control contribution comparison.

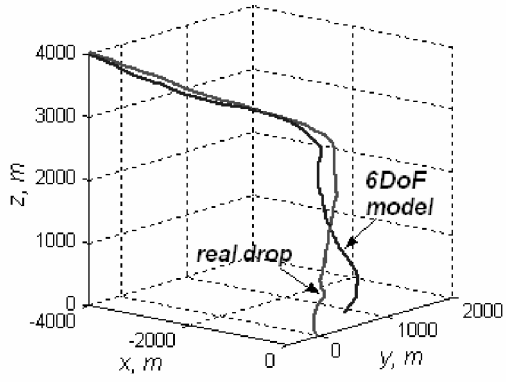

Fig. 25 Final comparison.

Clearly results obtained in simulation approximate flight-test data very well.

Final values of optimization parameters are shown in Table 4.

Conclusions

The paper presents results of the development of a six-DoF model of the controlled circular parachute. Key contributions of the paper include the following: 1) controlled model of the six-DoF circular parachute based on detailed modeling of the ADS geometry and utilization of the actuators performance data provided by the manufacturer; and 2) successful application of the two-step nonlinear system identification algorithm to refine the analytical values of the aerodynamic coefficients based on available flight-test data.

The resulting model acquitted itself well when compared with the flight-test data. However, further improvement is possible. It includes involving more optimization parameters into the model identification procedure. For instance, rather than finding averaged values of the aerodynamic force coefficients the effect of zero, one, and two risers activation might be addressed separately. Optimization parameters can also cover coefficients of the apparent mass tensor terms as a function of the angle of attack and canopy shape while applying control inputs $k_{mn} = k_{mn}(\bar{l}, n)$. More complex cost function (adequacy criterion) or even multiple criteria might be considered also. Further analysis could also include controlled ADS asymmetry, meaning the accounting of more terms in the inertia and apparent mass tensors.

Appendix: Geometry and Masses of the G-12-Based Aerial Delivery System

Tables A1–A3 contain geometric and mass data used to estimate the position of static mass center, the moments of inertia (Table A4), and arms of corresponding forces while computing moments acting on the generic G-12-based ADS.

Table A1 ADS components' dimensions

Component	Value
Length of suspension lines l_{SL}, m	15.55
Length of pressurized PMA l_{PMA}, m	5.80
Length of vented PMA l^*_{PMA}, m	7.62
Radius of uninflated canopy R_0, m	9.75
Radius of inflated canopy $R_p = \frac{2}{3}R_0$, m	6.50
Canopy shape ratio ε	0.82
Cone half-angle γ, deg	15.31
Dimension of a cubic payload container a_{pl}, m	1.22

Table A2 ADS components' masses

i	Component	Mass, kg
1	Canopy m_1	22.8
2	Suspension lines m_2	35.3
3	Four PMAs m_3	13.4
4	Payload m_4	990.0
——	**ADS total**	**1061.5**

Table A3 Auxiliary geometric relations

z coordinate of a specific point	Value, m
Centroid of hemispheroidal canopy z_1	−2.76
Centroid of suspension lines z_2	7.50
Centroid of PMAs z_3	17.80
Centroid of payload z_4	21.20
Static mass center of the whole ADS z_G	20.19
Center of pressure $z_P = -\frac{3}{8}\varepsilon R_p$	−2.00

Table A4 Moments of inertia, kg · m^2

i	Component	$\tilde{I}^i_{aa} = \tilde{I}^i_{bb}$	$I^i_{xx} = I^i_{yy}$	$I^i_{zz} = \tilde{I}^i_{cc}$
1	Canopy	365.93	539.16	623.98
2	SLs	1,047.09	3,032.22	770.76
3	PMAs	53.43	4,296.81	36.98
4	Payload	245.59	445,287.93	245.59
——	**ADS total**	——	**453,156.13**	**1,677.30**

Acknowledgments

Authors are grateful to R. Benney of the U.S. Army Soldier and Biological Chemical Command and to S. Dellicker of the U.S. Army Yuma Proving Ground (YPG) for their generous support as well as to the personnel of the YPG for providing the flight-test data. They also thank their colleagues I. Kaminer and R. Howard at the U.S. Naval Postgraduate School and V. Drozd at the Irvin Aerospace Canada for stimulating technical discussions.

References

[1]Henn, H., "Die Absinkeigenschaften von Fallschirmen (Descent Characteristics of Parachutes)," *Untersuchungen und Mitteilungen*, No. 6202, ZWB, Berlin, 1944 (in German); also Royal Aeronautical Establishment, Translation No. 223.

[2]Ludwig, R., and Heins, W., "Theoretische Untersuchungen zur Dynamischen Stabilität von Fallschirmen (Theoretical Study of the Dynamic Stability of Parachutes)," *Jahrbuch der Wissenschaftlichen Gesellschaft für Luft- und Raumfahrt*, 1962, pp. 224–230 (in German); also Faraday Translation, Nov. 1964.

[3]Lester, W. G. S., "A Note on the Theory of Parachute Stability," *Aeronautical Research Council, Reports and Memoranda*, No. 3352, London, 1962.

[4]Ibrahim, S., "Apparent Mass and Moment of Inertia of Cup-Shaped Bodies in Unsteady Incompressible Flow," Ph.D. Dissertation, Univ. of Minnesota, Twin Cities, 1965.

[5]Ibrahim, S., "Experimental Determination of the Apparent Moment of Inertia of Parachutes," Rept. FDL-TDR-64-153, Wright–Patterson AFB, April 1965.

[6]Wolf, D. F., "The Dynamic Stability of a Non-Rigid Parachute and Payload System," Ph.D. Dissertation, Univ. of Rhode Island, Kingston, 1968.

[7]Wolf, D. F., "An Investigation of Parachute Dynamic Stability," M.S. Thesis, Univ. of Rhode Island, Kingston, 1965.

[8]White, F. M., and Wolf, D. F., "A Theory of Three-Dimensional Parachute Dynamic Stability," *Journal of Aircraft*, Vol. 5, No. 1, 1968, pp. 86–92.

[9]Shilov, A. A., "Ob Ustoychivosti Dvizhenija Parachuta na Rezhime Ustanovivshegosja Snizhenija (The Stability of Motion of Parachute in the Steady-State Reduction Mode)," *Uchenie Zapiski TsAGI*, Vol. 2, No. 4, 1971, pp. 76–83 (in Russian); translation FTD-MT-24-0465-75.

[10]Byushgens, A. G., and Shilov, A. A., "Dinamicheskaja Model' Parachuta i Opredelenie ego Charakteristik (The Dynamic Model of Parachute and Determination of its Characteristics)," *Uchenie Zapiski TsAGI*, Vol. 3, No. 4, 1972, pp. 49–58 (in Russian); translation FTD-MT-24-0551-75.

[11]Shilov, A. A., "Analiz Ploskikh Slabo-Dempfirovannikh Oszilljaziy Parachuta v Svobodnom Ustanovivshemsja Snizhenii (An Analysis of the Plane Slightly Damped Oscillation of a Parachute in Free Steady Descent)" *Uchenie Zapiski TsAGI*, Vol. 4, No. 1, 1973, pp. 137–143 (in Russian); translation FTD-MT-24-0510-75.

[12]Tory, C., and Ayres, R., "Computer Model of a Fully Deployed Parachute," *Journal of Aircraft*, Vol. 14, No. 7, 1977, pp. 675–679.

[13]Eaton, J. A., "Added Mass and the Dynamic Stability of Parachutes," *Journal of Aircraft*, Vol. 19, No. 5, 1982, pp. 414–416.

[14]Yavus, T., and Cockrell, D. J., "Experimental Determination of Parachute Apparent Mass and Its Significance in Predicting Dynamic Stability," *Proceedings of 7th AIAA Aerodynamic Decelerator and Balloon Technology Conference*, AIAA, New York, 1981.

[15]Yavuz, T., "Determining and Accounting for a Parachute Virtual Mass," *Journal of Aircraft*, Vol. 26, No. 5, 1989, pp. 432–437.

[16]Cockrell, D. J., and Doherr, K.-F., "Preliminary Consideration of Parameter Identification Analysis from Parachute Aerodynamic Flight-Test Data," *Proceedings of 7th AIAA Aerodynamic Decelerator and Balloon Technology Conference*, AIAA, New York, 1981.

[17]Doherr, K.-F., and Saliaris, C., "On the Influence of Stochastic and Acceleration Dependent Aerodynamic Forces on the Dynamic Stability of Parachutes," *Proceedings of 7th AIAA Aerodynamic Decelerator and Balloon Technology Conference*, AIAA, New York, 1981.

[18]Doherr, K.-F., and Saliaris, C., "Dynamic Stability Analysis of Parachutes," CCG-U of M Course on Parachute Systems Technology, Oberpfaffenhofen, 1987.

[19]Doherr, K.-F., and Schilling, H., "Nine-Degree-of-Freedom Simulation of Rotating Parachute Systems," *Journal of Aircraft*, Vol. 29, No. 5, 1992, pp. 774–781.

[20]Cockrell, D. J., and Haidar, N. I. A., "Influence of the Canopy-Payload Coupling on the Dynamic Stability in Pitch of a Parachute System," *Proceedings of 12th RAeS/AIAA Aerodynamic Decelerator Systems Technology Conference and Seminar*, AIAA, London, May 1993.

[21]Dellicker, S., "Low Cost Parachute Navigation Guidance and Control," M.S. Thesis, U.S. Naval Postgraduate School, Monterey, CA, 1999.

[22]Williams, T., "Optimal Parachute Guidance, Navigation, and Control for the Affordable Guided Airdrop System (AGAS)," M.S. Thesis, U.S. Naval Postgraduate School, Monterey, CA, 2000.

[23]Johnson, J., Yakimenko, O., Kaminer, I., and Dellicker, S., "On the Development and Pre-Flight Testing of the Affordable Guided Airdrop System for G-12 Cargo Parachute," *Proceedings of 16th AIAA Aerodynamic Decelerator Systems Technology Conference and Seminar*, AIAA, Reston, VA, 2001.

[24]"Precision Airdrop Technology Conference and Demonstration," Final Rept. 02-019, DTC Project 8-ES-065-G12-002, Yuma, AZ, 2001, URL:http://yuma-notes1.army.mil/mtea/patcadreg.nsf.

[25]Mosseev, Yu., "Fluid-Structure Interaction Simulation of the U.S. Army G-12 Parachute," Rept. 17-01-RDD Ozon, Moscow, Russia, 2001, URL: http://www.mtu-net.ru/mosseev/rd.htm.

[26]Knacke, T. W., *Parachute Recovery Systems Design Manual*, Para Publishing, Santa Barbara, CA, 1992.

[27]Benney, R., Brown, G., and Stein, K., "A New Pneumatic PMA: Its Use in Airdrop Applications," *Proceedings of 15th CAES/AIAA Aerodynamic Decelerator Systems Technology Conference*, AIAA, Reston, VA, 1999.

[28]Etkin, B., *Dynamics of Flight*, Wiley, New York, 1959.

[29]Schmidt, L., *Introduction to Aircraft Flight Dynamics*, AIAA, Reston, VA, 1998.

[30]Tuma, J. J., *Engineering Mathematics Handbook*, McGraw–Hill, New York, 1987.

[31]Favorin, M. V., *Momenti Inerzii Tel. Spravochnik (Moments of Inertia of Bodies. Reference Book)*, Mashinostroenie, Moscow, 1977 (in Russian).

[32]Ljung, L., *System Identification: Theory for the User*, Prentice–Hall, Upper Saddle River, NJ, 1999.

[33]Marple, S. L., *Digital Spectral Analysis*, Prentice–Hall, Upper Saddle River, NJ, 1987.

[34]Rotea, M. A., and Kothandaraman, G., "Parameter Estimation for Airdrop System: Final Report," Univ. of Purdue, Contract 00244-00-P-3258, IL, 2001.

[35]Yakimenko, O., Dobrokhodov, V., Johnson, J., Kaminer, I., Dellicker, S., and Benney, R., "On Control of Autonomous Circular Parachutes," *Proceedings of the AIAA Guidance, Navigation, and Control Conference*, AIAA, Reston, VA, 2002.